Hollowness in pp and $p\bar{p}$ scattering in a Regge model

Wojciech Broniowski,[1,2,*] László Jenkovszky,[3,†] Enrique Ruiz Arriola,[4,‡] and István Szanyi[5,§]

[1]*The H. Niewodniczański Institute of Nuclear Physics, Polish Academy of Sciences, 31-342 Cracow, Poland*

[2]*Institute of Physics, Jan Kochanowski University, 25-406 Kielce, Poland*

[3]*Bogolyubov Institute for Theoretical Physics (BITP), Ukrainian National Academy of Sciences 14-b Metrologicheskaya strasse, Kiev, 03680, Ukraine*

[4]*Departamento de Física Atómica, Molecular y Nuclear and Instituto Carlos I de Fisica Teórica y Computacional, Universidad de Granada, E-18071 Granada, Spain*

[5]*Uzhgorod National University, 14 Universytets'ka strasse, Uzhgorod, 88000, Ukraine*

(Received 12 June 2018; published 16 October 2018)

The proton-proton and proton-antiproton inelasticity profiles in the impact parameter display very interesting and sensitive features which cannot be deduced solely from the current large body of high-energy scattering data. In particular, phenomenological studies exhibit a link between the ratio of the real to imaginary parts of the elastic scattering amplitude at a finite momentum transfer, and the corresponding change of character of the inelastic processes from central to peripheral collisions. We describe how a theoretical model, accommodating the existing data, based on the Regge hypothesis including both the Pomeron and odderon as double poles, and ω and f mesons as single poles in the complex-J plane, generates a hollow in the inelasticity at low impact parameters. The hollowness effect, which generally may be sensitive to model details, does unequivocally take place both for pp and $p\bar{p}$ collisions within the applied Regge framework, indicating inapplicability of inelasticity-folding geometric approaches.

DOI: 10.1103/PhysRevD.98.074012

I. INTRODUCTION

Scattering experiments with hadrons are usually designed to learn about their structure and interactions [1]. In the case of proton-proton (pp) and proton-antiproton ($p\bar{p}$) collisions, a wealth of differential elastic scattering data has been collected since the mid 1950s above center-of-mass (CM) energies of $\sqrt{s} = 6$ GeV, characterized by elastic diffractive scattering. Accordingly, the data exhibit a peak at soft kinematics, i.e., at small momentum transfers $-t \ll s$ (for recent comprehensive reviews of the data and models see, e.g., [2,3]). Despite the abundant experimental information and numerous theoretical efforts, it is fair to say that we lack a truly working approach based directly on the fundamental quantum chromodynamics (QCD) in the nonperturbative soft regime $-t \lesssim \Lambda^2_{\rm QCD} \ll s$. This situation has stimulated the use of pre-QCD ideas and models which embody not only the desirable theoretical constraints such as unitarity, crossing, and analyticity, but also display the outstanding experimental features of the data. These models and the following parametrizations have been steadily and quantitatively tested and improved along the years. Regge theory, while phenomenological and not fundamental from the QCD viewpoint, satisfies these important theoretical constraints and at the same time is flexible enough as to allow for a uniform quantitative description of the data.

A complementary and enlightening way of visualizing the high-energy scattering results is by passing, via the Fourier-Bessel transform, from the momentum transfer t to the impact parameter b. This variable is conjugate to $\sqrt{-t}$, with $b \sim 1/\sqrt{-t}$. In 1963 van Hove introduced the inelasticity profile or the overlap function [4,5] (see also [6] and the references therein), which corresponds to the impact parameter distribution of the inelastic cross section. This representation has a transparent interpretation, since different impact parameters decouple from one another. A major issue in this regard is the fact that the inelastic profile depends on the phase of the scattering amplitude and thus is not determined solely from the differential elastic scattering cross section *without* some additional assumptions. Despite this generic source of arbitrariness, most pp analyses in the wide range of 10 GeV $\le \sqrt{s} \le$ 500 GeV have provided a shape for the inelasticity profile which is compatible with a

*Wojciech.Broniowski@ifj.edu.pl
†jenk@bitp.kiev.ua
‡earriola@ugr.es
§sz.istvan03@gmail.com

natural expectation that the most inelastic collisions are central, i.e., the inelasticity profiles have a maximum at $b = 0$.

Whereas this central maximum of inelasticity is in fact explicitly implemented in geometric models [7–12] which are quite naturally based on folding of partonic distributions in the impact parameter space, there is no particular *a priori* reason why it should be so. In fact, recent papers [13–25] have reported a mounting evidence suggesting that this paradigm may change in the light of the measurements by the TOTEM collaboration at the CERN Large Hadron Collider (LHC). The found *hollowness* feature shows that the inelasticity profile becomes maximal at a finite value of b, whereas at $b = 0$ it has a local minimum.

In this paper we reanalyze this issue in a simple Regge model which, as will be shown, provides efficiently a reasonable description of a large pp and $p\bar{p}$ elastic scattering data in the range $10\ \text{GeV} \leq \sqrt{s} \leq 13\ \text{TeV}$. The main advantage of the Regge framework is that it not only predicts the s dependence at small t, but also fixes the total amplitude, and hence a fit to the elastic differential cross section allows one to determine both the modulus and the argument of the amplitude. Of course, there are many Regge models on the market, so the question of uniqueness of the description is a pertinent one; we leave a thorough comparison of different model proposals and parametrizations for a future research and here focus on a particularly simple Regge model.

II. THE BASICS

In this section we introduce our notation and methodology in a way that our problem can be easily stated, and motivate in passing our use of the Regge theory within this context. In general, the NN and $N\bar{N}$ elastic scattering amplitudes have 5 independent complex components which can only be determined from a complete set of experiments involving 9 observables, such as differential cross sections and polarization data [26]. The amplitudes fulfill the crossing relations [27,28]. As is customary in such studies, we neglect the spin dependence. Whereas the degree of uncertainty introduced by this approximation is not known, the spin-flip amplitudes have been found to be nonvanishing but small in E950 fixed target experiment at $\sqrt{s} \sim 25$ GeV at the BNL Relativistic Heavy-Ion Collider (RHIC) (for a review see, e.g., [29] and references therein). Thus a small but systematic error in the amplitude is foreseen. This is an important observation for the statistical analysis of the data which allows for a more relaxed interpretation of the χ^2 minimization than the conventional one, as will be used in Sec. III.

A. The phase ambiguity

An important issue which is of relevance in our analysis regards the uniqueness of the amplitude obtained from the differential cross section via fitting analysis in the presence of absorption, as it is the case for pp and $p\bar{p}$ scattering at $t < 0$ and $s > 4M^2$, with M denoting the proton mass. Indeed, if $f(s,t)$ is the elastic scattering amplitude,

$$f(s,t) = \mathrm{Re}\, f(s,t) + i\, \mathrm{Im} f(s,t) \tag{1}$$

the invariant differential elastic cross section is given by

$$\frac{d\sigma_{el}}{dt} = \frac{\pi}{p^2} |f(s,t)|^2, \tag{2}$$

where $p = \sqrt{s/4 - M^2}$ denotes the CM momentum of the proton. Only the absolute value $|f(s,t)|$ enters Eq. (2), thus in the notation

$$f(s,t) = |f(s,t)| \frac{\rho(s,t) + i}{\sqrt{1 + \rho(s,t)^2}} \tag{3}$$

the real function $\rho(s,t)$, defined as

$$\rho(s,t) = \frac{\mathrm{Re} f(s,t)}{\mathrm{Im} f(s,t)} \tag{4}$$

remains unconstrained by the elastic scattering data alone. This freedom merely reflects the incomplete information on the system. Of course, the (s,t) dependent phase of the scattering amplitude is not arbitrary and has a physical significance [30] (for a review see, e.g., [31]).

In quantum mechanics, this ambiguity is resolved by analyticity in the scattering potential at a fixed distance. Likewise, the fixed-t dispersion relations have been suggested as a possible way to circumvent the ambiguity problem in pp or $p\bar{p}$ scattering, since they impose analyticity in the s variable for the scattering amplitude $f(s,t)$. Thus, up to subtractions (which may depend on t), the real and imaginary parts are related to each other via the dispersion relation

$$\mathrm{Re} f(s,t) = \frac{1}{\pi} \int_{4M^2}^{\infty} ds' \frac{\mathrm{Im} f(s',t)}{s' - s}. \tag{5}$$

For $t = 0$ one has the optical theorem

$$\mathrm{Im} f(s,0) = \frac{p}{4\pi} \sigma_{\mathrm{tot}}(s). \tag{6}$$

If one uses the crossing-odd variable

$$\nu = \frac{s - u}{4M} = \frac{2s - t - 4M^2}{4M}, \tag{7}$$

one has the crossing relation $f_{pp}(\nu,t) = f_{p\bar{p}}(-\nu,t)^*$ [27,28] for the central interaction. In the limit $s \ll t$, it yields $f_{pp}(s,t) = f_{p\bar{p}}(-s,t)^*$, such that one can write a fixed-t dispersion relation for the odd and even

combinations, $f_{\pm}(s,t) = f_{p\bar{p}}(s,t) \pm f_{pp}(s,t)$, independently. In this limit, and neglecting the threshold effect which can be done at large s, the family of functions $\beta(t)s^{\alpha(t)}$ fulfills Eq. (5), since for $-1 < \alpha < 0$ one has the identity

$$\frac{1}{\pi}\int_0^\infty ds' s'^{\alpha}\left[\frac{1}{s'-s} \pm \frac{1}{s'+s}\right] = \frac{(-s)^\alpha \pm (s)^\alpha}{\sin \pi\alpha}. \quad (8)$$

Here we take $-s = |s|e^{i\pi}$ and proceed by analytic continuation, making the necessary subtractions for other values of α. Therefore, the Regge theory, where the amplitude reads $f(s,t) = \sum_i \beta_i(t)s^{\alpha_i(t)}$, does indeed satisfy the fixed-t dispersion relations for $s \ll t$. The Regge amplitude is odd under crossing $pp \to p\bar{p}$.[1] These features justify our motivation to take a particular phenomenologically based realization of a Regge theory in the following sections.

B. Impact parameter and the overlap function

The Fourier-Bessel transform of the amplitude $f(s,t)$ is denoted as $ph(b,s)$ [6], with p denoting the CM momentum of the proton,

$$2ph(b,s) = 2\int_0^\infty qdqJ_0(bq)f(s,-q^2). \quad (9)$$

Next, we present a glossary of formulas for the total, elastic, and inelastic cross sections in the b representation:

$$\sigma_{\rm tot}(s) = 4p\int d^2b \mathrm{Im}h(b,s), \quad (10)$$

$$\sigma_{\rm el}(s) = 4p^2\int d^2b|h(b,s)|^2, \quad (11)$$

$$\sigma_{\rm in}(s) \equiv \sigma_{\rm tot}(s) - \sigma_{\rm el}(s) = \int d^2b\sigma_{\rm in}(b,s). \quad (12)$$

Here, the dimensionless integrands $\sigma_{\rm tot}(b,s)$, $\sigma_{\rm el}(b,s)$, and $\sigma_{\rm in}(b,s)$ can be interpreted as profiles representing the b-dependent relative number of the appropriate collisions. The inelasticity profile is equal to

$$\sigma_{\rm in}(b,s) = 4p\mathrm{Im}h(b,s) - 4p^2|h(b,s)|^2. \quad (13)$$

Unitarity and positivity of absorption imply

$$1 \geq \sigma_{\rm in}(b,s) \geq 0, \quad (14)$$

whereas the condition

$$\sigma_{\rm in}(b,s) \leq 2(2p\mathrm{Im}h(b,s)) - (2p\mathrm{Im}h(b,s))^2 \quad (15)$$

yields, consistently, the upper bound $\sigma_{\rm in}(b,s) \leq 1$.

The criterion for hollowness is to have a minimum of $\sigma_{\rm in}(b,s)$ at $b = 0$, i.e.,

$$\left.\frac{d\sigma_{\rm in}(b,s)}{db^2}\right|_{b=0} < 0. \quad (16)$$

At this point it should be noted that the phase ambiguity discussed in Sec. II is transferred to the impact parameter space, hence the very issue of hollowness cannot be decided based just on the elastic scattering data, without further theoretical or model input. In fact, in [32] it has been shown that adopting various admissible choices of $\rho(s,t)$ influences quantitatively and qualitatively the result.

C. The exponential fall-off and hollowness

The most characteristic feature of the high-energy elastic scattering is the diffraction peak, which is characterized by the slope parameter at the origin, defined as

$$B(s) = \frac{d}{dt}\ln\left.\frac{d\sigma_{el}(s,t)}{dt}\right|_{t=0}. \quad (17)$$

A simple Gaussian profile in the momentum transfer [note an assumed t-independent $\rho(s)$ function]

$$f(s,t) = \frac{p\sigma_{\rm tot}(s)}{4\pi}[i+\rho(s)]e^{B(s)t/2} \quad (18)$$

fulfills the optical theorem. In the $-t \ll s$ limit, one has

$$\sigma_{\rm el}(s) = \int_{-s+4M^2}^0 (-dt)\frac{d\sigma_{\rm el}}{dt}(s,t) \to \int_{-\infty}^0 (-dt)\frac{d\sigma_{\rm el}}{dt}(s,t) \quad (19)$$

and the following equation is satisfied:

$$\frac{\sigma_{\rm el}(s)}{\sigma_{\rm tot}(s)} = \frac{[1+\rho(s)^2]\sigma_{\rm tot}(s)}{16\pi B(s)}. \quad (20)$$

This relation has been observed to work quite accurately in a soft-Pomeron pp and $p\bar{p}$ model for a fit range of 5 GeV $< \sqrt{s} <$ 500 GeV [33]. The model applied in Sec. III also fulfills relation (20) to an accuracy better than 5% in the whole fitting range.

The Fourier-Bessel transform of the exponential profile (18) is

$$2ph(b,s) = \frac{\sigma_{\rm tot}(s)}{4\pi B}[i+\rho(s)]e^{-b^2/2B}. \quad (21)$$

Substitution of this form into Eq. (13) at $b = 0$ implies, via the positivity condition (14), that

[1]This in particular refers to single Regge poles, but it is also valid for derivatives with respect to α which arise for the n-fold Regge poles, see Sec. III.

$$\sigma_{\rm el}(0,s)=\frac{\sigma_{\rm tot}(s)}{4\pi B}\left[2-4\frac{\sigma_{\rm el}(s)}{\sigma_{\rm tot}(s)}\right]\geq 0, \tag{22}$$

and thus

$$\sigma_{\rm el}(s)\leq\frac{1}{2}\sigma_{\rm tot}(s), \tag{23}$$

in accordance with experiment. Thus, in the Gaussian model the *largest* elastic cross section which can be achieved is half of the total cross section, which shows that the scattering in this model is intrinsically inelastic.

In order to better appreciate this point, it is worth to consider a situation for an arbitrary inelasticity profile, however, with a sharp edge at, say, $b=R$,

$$2ph(b,s)=0, \qquad b\geq R. \tag{24}$$

Thus, we have

$$\begin{aligned}\sigma_{\rm in}&=\int_0^R 2\pi b db[4p\,{\rm Im}h(b,s)-4p^2|h(b,s)|^2],\\ \sigma_{\rm tot}&=\int_0^R 2\pi b db[4p\,{\rm Im}h(b,s)].\end{aligned} \tag{25}$$

Our goal is to *maximize* $\sigma_{\rm in}$ for a general complex profile $h(b,p)$ with a *fixed* $\sigma_{\rm tot}$ which can be readily done by maximizing

$$\max_{h(p,s)}[\sigma_{\rm in}-\lambda\sigma_{\rm tot}], \tag{26}$$

with λ a Lagrange multiplier. We get from the corresponding Euler-Lagrange equations ${\rm Re}h(p,s)=0$, and thus

$$1-\lambda-2p{\rm Im}h(b,s)=0, \tag{27}$$

which implies a *constant* profile. For such a situation, the *smallest* possible elastic cross section is $\sigma_{\rm el}=\sigma_{\rm tot}/2$ with a black-disk geometry $\sigma_{\rm in}(b,s)=1$ for $b\leq R$, yielding $\sigma_{\rm in}(s)=\pi R^2$. Therefore, if $\sigma_{\rm el}(s)<\sigma_{\rm tot}(s)/2$, as happens experimentally, the edge cannot be sharp and a gray disk picture sets in.

Turning to the Gaussian profile, the curvature of the inelasticity profile at the origin is

$$\frac{1}{2}\frac{d^2\sigma_{\rm in}(b,s)}{db^2}\bigg|_{b=0}=\frac{64\pi\sigma_{\rm el}^2(4\sigma_{\rm el}(s)-\sigma_{\rm tot}(s))}{(\rho(s)^2+1)^2\sigma_{\rm tot}(s)^4}, \tag{28}$$

such that the turnover to hollowness takes place at [32]

$$\frac{\sigma_{\rm el}(s)}{\sigma_{\rm tot}(s)}=\frac{1}{4}, \tag{29}$$

a fact that will also follow to a good accuracy in the more sophisticated Regge model discussed in Sec. III.

III. THE DIPOLE REGGE MODEL

One of the most remarkable successes of the Regge theory was the early prediction of a diffraction pattern in high energy collisions [1]. However, the conventional Regge theory based on single Regge poles in the complex-J plane does not account easily for the dip or the bump structures unveiled in the CERN Interacting Storage Rings (ISR) experiments (see, e.g., [6] and references therein), hence modifications became mandatory. The Barger and Phillips empirical parametrization [34], which was successful in fitting the early data and was improved recently by the inclusion of form factors [35], does not provide an energy dependence stemming from Regge ideas, and hence does not comply to the fixed-t dispersion relations.

However, as noted many years ago, multiple Regge poles are not only not forbidden, but may in fact naturally occur quantum mechanically [36,37]. They are actually suggested by the dual models with the Mandelstam analyticity (see, e.g., [38] for an impact parameter analysis). The model with different Regge trajectories, including the double-pole odderon, was thus proposed [39] and later extended for finite t [40] and the odderon rise [41,42]. The upgraded version was described in [43].

Let us mention in this regard that whereas the order of the Regge pole cannot be fixed by first principles, the Froissart bound prevents poles or order higher than 3, and the requirement $\sigma_{\rm el}\leq\sigma_{\rm tot}$ prevents asymptotically a moving triple pole [44].

In the light of the recent TOTEM measurements at $\sqrt{s}=13$ TeV, the double pole Pomeron is preferred compared to a single- or triple-pole Pomeron [45]. The statement is based on dispersion relations for the meson-proton and proton-proton forward elastic scattering. Recent data from the TOTEM Collaboration at 13 TeV provide a convincing evidence on the existence of the odderon [46], discarding many of the models on the market not including this particular element. Further successful fits were proposed in [47–49].

In this paper, we consider the spin-averaged case of the invariant high-energy scattering amplitudes, which are sums of four terms [43]. The two asymptotically leading terms are the Pomeron (P) and the odderon (O), and two secondary contributions come from the f and ω Regge poles.

We note that P and f have positive C, thus enter the scattering amplitude with the same sign in pp and $p\bar{p}$ scattering, whereas O and ω have negative C, thus enter with opposite signs[2]:

$$A(s,t)_{pp}^{p\bar{p}}=A_P(s,t)+A_f(s,t)\pm[A_\omega(s,t)+A_O(s,t)]. \tag{30}$$

[2]Here we use the normalization where $\frac{d\sigma_{\rm el}}{dt}(s,t)=\frac{\pi}{s^2}|A(s,t)|^2$ and $\sigma_{\rm tot}(s)=\frac{4\pi}{s}{\rm Im}A(s,t=0)$.

The model of Eq. (30) may be extended by adding more Reggeons, whose role becomes increasingly important towards lower energies. In our fits at relatively large s, their contribution can be effectively absorbed in f and ω [50].

Secondary Reggeons are parametrized in a standard way [50,51], with linear Regge trajectories and exponential residua. The f and ω Reggeons are the principal nonleading contributions to pp or $p\bar{p}$ scattering:

$$A_f(s,t) = a_f e^{-i\pi\alpha_f(t)/2} e^{b_f t}(s/s_{0f})^{\alpha_f(t)}, \tag{31}$$

$$A_\omega(s,t) = i a_\omega e^{-i\pi\alpha_\omega(t)/2} e^{b_\omega t}(s/s_{0\omega})^{\alpha_\omega(t)}, \tag{32}$$

with $\alpha_f(t) = \alpha_{0f} + \alpha'_f t$ and $\alpha_\omega(t) = \alpha_{0\omega} + \alpha'_\omega t$.

As already mentioned, the Pomeron is a dipole in the J-plane

$$\begin{aligned} A_P(s,t) &= \frac{d}{d\alpha_P}[e^{-i\pi\alpha_P/2} G(\alpha_P)(s/s_{0P})^{\alpha_P}] \\ &= e^{-i\pi\alpha_P(t)/2}(s/s_{0P})^{\alpha_P(t)} \\ &\quad \times [G'(\alpha_P) + (L_P - i\pi/2)G(\alpha_P)]. \end{aligned} \tag{33}$$

Since the first term in squared brackets determines the shape of the cone, one fixes

$$G'(\alpha_P) = -a_P e^{b_P[\alpha_P - 1]}, \tag{34}$$

where $G(\alpha_P)$ is recovered by integration. Consequently, the Pomeron amplitude of Eq. (33) may be rewritten in the following "geometric" form (for details see [52] and references therein):

$$\begin{aligned} A_P(s,t) = i\frac{a_P s}{b_P s_{0P}}[r^2_{1P}(s) e^{r^2_{1P}(s)[\alpha_P - 1]} \\ - \varepsilon_P r^2_{2P}(s) e^{r^2_{2P}(s)[\alpha_P - 1]}], \end{aligned} \tag{35}$$

where $r^2_{1P}(s) = b_P + L_P - i\pi/2$, $r^2_{2P}(s) = L_P - i\pi/2$, $L_P \equiv \ln(s/s_{0P})$, and the Pomeron trajectory is

$$\alpha_P \equiv \alpha_P(t) = 1 + \delta_P + \alpha'_P t. \tag{36}$$

The odderon contribution (labeled with the subscript "O") is assumed to be of the same form as for the Pomeron, apart for different values of the adjustable parameters:

$$\begin{aligned} A_O(s,t) = \frac{a_O s}{b_O s_{0O}}[r^2_{1O}(s) e^{r^2_{1O}(s)[\alpha_O - 1]} \\ - \varepsilon_O r^2_{2O}(s) e^{r^2_{2O}(s)[\alpha_O - 1]}], \end{aligned} \tag{37}$$

where $r^2_{1O}(s) = b_O + L_O - i\pi/2$, $r^2_{2O}(s) = L_O - i\pi/2$, $L_O \equiv \ln(s/s_{0O})$, and the trajectory is

$$\alpha_O \equiv \alpha_O(t) = 1 + \delta_O + \alpha'_O t. \tag{38}$$

The free parameters of the model were simultaneously fitted to the data on the differential elastic pp and $p\bar{p}$ cross section, as well as to the data on the total cross section and the ratio

$$\rho(s) = \frac{\mathrm{Re}A(s,t=0)}{\mathrm{Im}A(s,t=0)}. \tag{39}$$

The fit was done by using the MIGRAD algorithm of MINUIT 2 with the data in the following intervals:

(i) for pp differential elastic cross section at 7 TeV [53]: 0.35 GeV$^2 \le -t \le 2.5$ GeV^2;
(ii) for $p\bar{p}$ differential elastic cross section at 546 and 630 GeV [54]: 0.5 GeV$^2 \le -t \le 2.5$ GeV^2;
(iii) for pp and $p\bar{p}$ total cross section and parameter ρ: 20 GeV $\le \sqrt{s} \le$ 57 TeV [53,55–61].

The above intervals in t were chosen to optimize our fit, whereby the number of the outliers in the differential cross section was reduced to 63. The optimum values of the fitted parameters and the values of χ^2 are collected in Table I. Figures 1–2 show the quality of the model fit to the world data. We note that the overall agreement catches all the features of the data. The value of $\chi^2/\mathrm{NDF} = 1.4$ indicates a

TABLE I. Optimum values and the uncertainties of the model parameters following from a joint fit to pp and $p\bar{p}$ data for elastic differential cross section, the total cross section, and the parameter ρ. See text for details.

Pomeron		Odderon		Reggeons	
$a_P[\sqrt{\mathrm{mb\,GeV^2}}]$	360 (fixed)	$a_O[\sqrt{\mathrm{mb\,GeV^2}}]$	1.75 ± 0.11	$a_f[\sqrt{\mathrm{mb\,GeV^2}}]$	-20.05 ± 0.17
b_P	4.19 ± 0.15	b_O	0.914 ± 0.007	$b_f[\mathrm{GeV}^{-2}]$	0 (fixed)
δ_P	0.0293 ± 0.0005	δ_O	0.275 ± 0.005	α_{0f}	0.703 (fixed)
$\alpha'_P[\mathrm{GeV}^{-2}]$	0.5069 ± 0.0028	$\alpha'_O[\mathrm{GeV}^{-2}]$	0.2309 ± 0.0017	$\alpha'_f[\mathrm{GeV}^{-2}]$	0.84 (fixed)
ε_P	0.278 ± 0.015	ε_O	1.318 ± 0.003	$s_{0f}[\mathrm{GeV}^2]$	1 (fixed)
$s_{0P}[\mathrm{GeV}^2]$	100 (fixed)	$s_{0O}[\mathrm{GeV}^2]$	100 (fixed)	$a_\omega[\sqrt{\mathrm{mb\,GeV^2}}]$	10.65 ± 0.64
				$b_\omega[\mathrm{GeV}^{-2}]$	0 (fixed)
				$\alpha_{0\omega}$	0.435 (fixed)
NDF = 159	$\chi^2 = 223.5$	$\chi^2/\mathrm{NDF} = 1.4$		$\alpha'_\omega[\mathrm{GeV}^{-2}]$	0.93 (fixed)
				$s_{0\omega}[\mathrm{GeV}^2]$	1 (fixed)

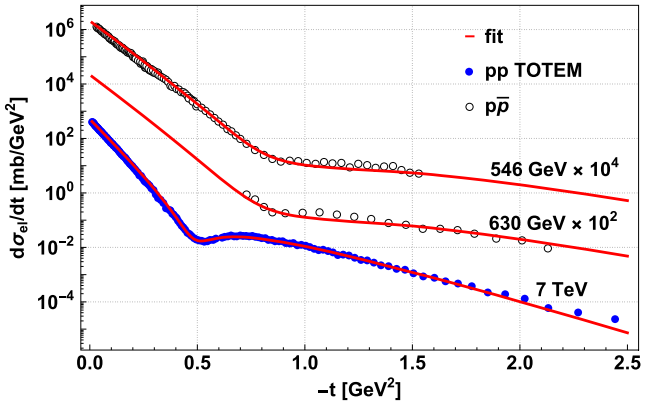

FIG. 1. Fit to the pp and $p\bar{p}$ differential elastic cross sections at several collision energies, plotted as a function of the momentum transfer $-t$, compared to the data of Refs. [53,54].

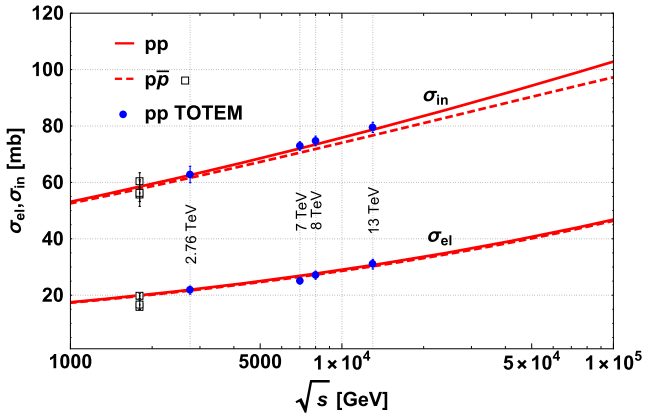

FIG. 3. Elastic and inelastic pp and $p\bar{p}$ cross sections, plotted as functions of $\sqrt{s}$ and compared to the data of Refs. [56–59]. The lines indicate our fit.

need for improvement on the theoretical model side, as remarked in Sec. II.

The results for $\sigma_{\rm el}(s)$ and $\sigma_{\rm in}(s)$ are shown in Fig. 3. The model elastic cross section $\sigma_{el}(s)$ is calculated by integration of our fit to $d\sigma_{\rm el}(s,t)/dt$. Again, we note a fair agreement with the experimental data.

Next, we pass to a discussion of the "anatomy" of the model, focusing on the role of its various components. In Fig. 4 we plot the absolute values of the pp and $p\bar{p}$ elastic scattering amplitudes and their components. At low $-t$ the Pomeron contribution is dominant, and at high $-t$ the odderon takes over, as is evident from the relation between the slopes of their trajectories, $\alpha'_P > \alpha'_O$, and the b-parameters. The interference of both P and O components shows up in the transition region around $-t = 0.5$ GeV^2, generating the dip. We note that the contribution of the mesonic Regge trajectories is negligible at the TOTEM collision energies and is essential only at low s.

In Fig. 5 we show the phase of the elastic amplitude, defined conventionally as $\pi/2 - \mathrm{Arg}[A_i(s,-t)]$. We note that the Pomeron determines the phases for both pp and $p\bar{p}$ at low values of $-t$. At high values of $-t$ the phase of $p\bar{p}$ is determined by the odderon, and the phase of pp is relatively shifted upwards by π, which simply reflects the relative sign between the odderon component of the two amplitudes.

IV. HOLLOWNESS ANALYSIS

As stated in the Introduction, in the present work we focus on the surprising feature of the pp (and $p\bar{p}$) scattering, the hollowness, which emerges at the LHC energies: the most inelastic collision become slightly peripheral, with $\sigma_{\rm in}(b,s)$ assuming a maximum at $b > 0$, and having a minimum at $b = 0$. In what follows we complement the balanced review of Ref. [19] and the

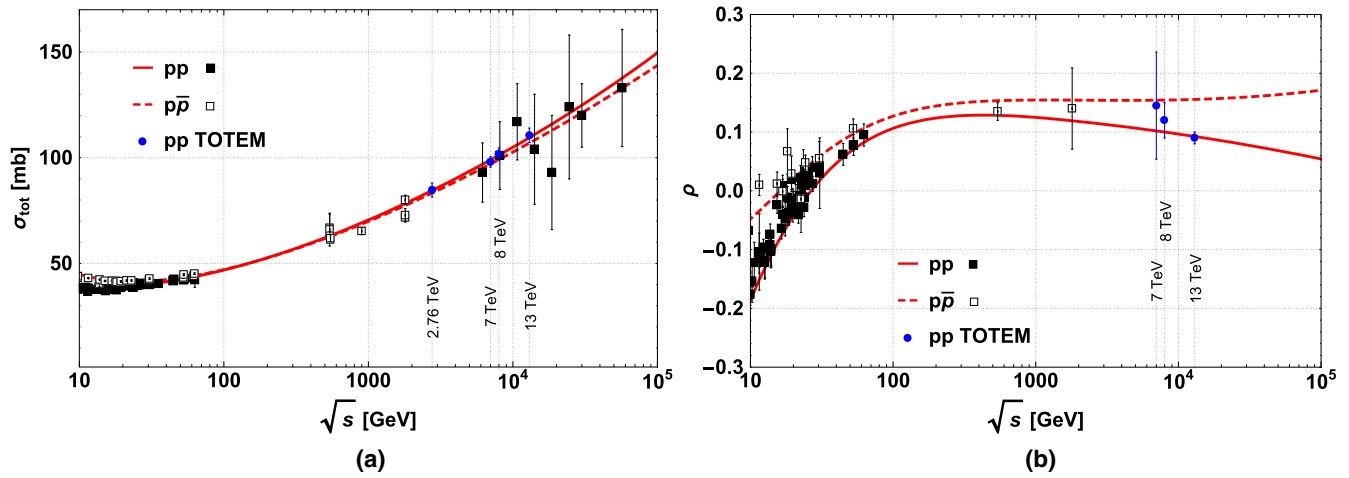

FIG. 2. (a): Total pp and $p\bar{p}$ cross sections plotted as a functions of $\sqrt{s}$, compared to the data of Refs. [55–59]. (b): The ratio of the real to imaginary part of the elastic pp and $p\bar{p}$ amplitude at $t = 0$, plotted as a function of $\sqrt{s}$ and compared to the data of Refs. [53,58,60,61]. The lines indicate our joint fit. The LHC collision energies are indicated with the vertical labels.

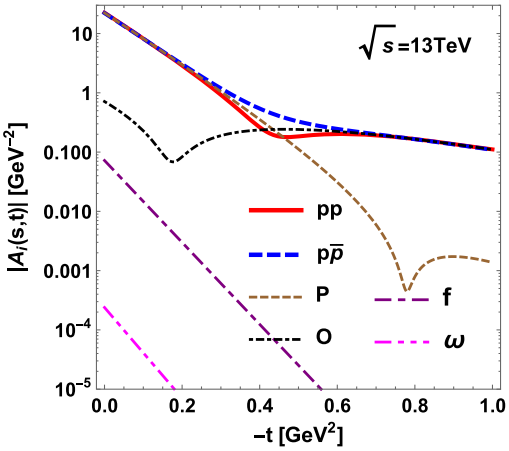

FIG. 4. Absolute values of the pp and $p\bar{p}$ elastic scattering amplitudes (thick lines), and absolute values of their components (thin lines), plotted as functions of $-t$ for the TOTEM collision energy of $\sqrt{s} = 13$ TeV. At low $-t$ the Pomeron dominates, whereas at high $-t$ the odderon dominates, and the interference of both components is manifest in the transition region around $-t = 0.5$ GeV^2. The contribution of the mesonic Regge trajectories is negligible at the TOTEM collision energies.

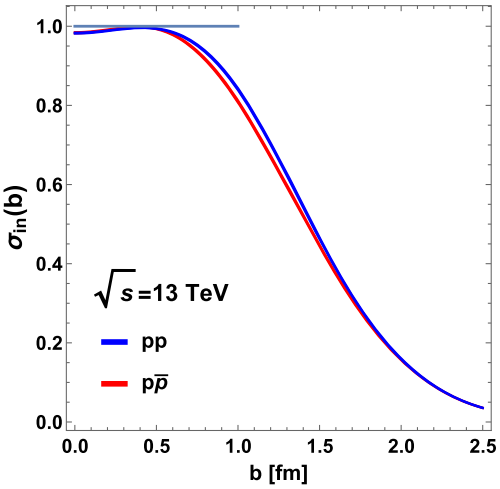

FIG. 6. The inelastic profiles $\sigma(b, s)$ for pp and $p\bar{p}$ collisions, plotted as functions of the impact parameter b for the TOTEM collision energy of $\sqrt{s} = 13$ TeV. We note the presence of the hollowness effect, somewhat stronger for $p\bar{p}$ than for pp. The uncertainty bands, following from the error propagation from our fit parameters, are within the thickness of the lines.

discussion in [20] with the results in the Regge model of Sec. III. The peripheral or central character of both the elastic and inelastic scattering was questioned in [62], where it was shown that the shape of the inelastic profile depends strongly on the phase of the elastic amplitude [63]. In a recent upgrade [64,65], a preference for more peripheral elastic than inelastic scattering is supported, based on a careful treatment of the Coulomb interaction and the corresponding strong phase (see, however, the critical remarks in [66], where a different formula for the strong phase is proposed). The shadowing and antishadowing scattering scenarios have been discussed together with the hollowness behavior in [67]. In addition, unitarization features also produce hollowness [68], based on the old scheme from Ref. [69].

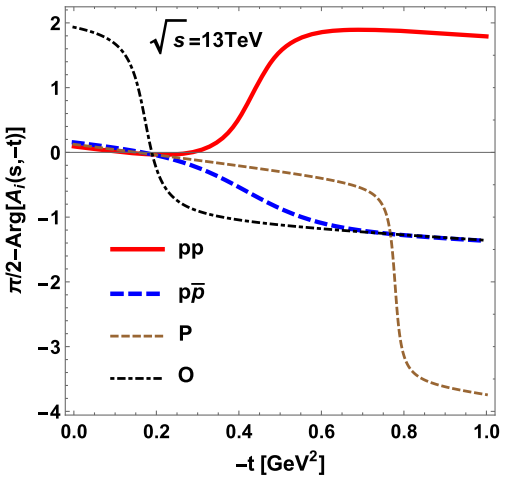

FIG. 5. Same as in Fig. 4 but for the phases, defined as $\pi/2 - \mathrm{Arg}[A_i(s, -t)]$. At low $-t$ the phases for both pp and $p\bar{p}$ are determined by the Pomeron, whereas at high $-t$ the phase of $p\bar{p}$ is determined by the odderon, while the phase of pp is shifted upwards by π.

A recent discussion of hollowness by two of the present authors (W.B. and E.R.A.) within an inverse scattering approach, where a distinction of the 2D- and 3D-hollowness was established [16,17,20,32], was based on empirical parametrizations [35,70,71]. These parametrizations qualify as means of fitting the data, but actually feature no particular theory or physical picture. We also point out that a rather flat behavior in the inelastic profile near $b = 0$ has been observed [72], which may be interpreted as a precursor of the 2D-hollowness and the occurrence of the 3D-hollowness [16,17,20,32]. Hollowness has also been reported to emerge from a hot-spot picture of the pp collision at the LHC energies [18].

In [32] we have shown that the existence of hollowness depends strongly on the t-dependence of the ρ parameter.[3] Once we recognize that hollowness cannot be deduced from present data alone, in this paper we take a different point of view, where we want to decide on the hollowness within a given theoretical framework.

In the following, we apply the formulas of Subsection II B to the model of Sec. III. We first look at the inelasticity profile $\sigma_{\mathrm{in}}(b, s)$, shown $\sqrt{s} = 13$ TeV in Figs. 6 and 7. We clearly

[3]The criticism that has been raised in Ref. [73] is based on an incorrect perception of the approximations involved and does not address the arbitrariness of the t-dependence of the $\rho(s, t)$ parameter, which is crucial for hollowness.

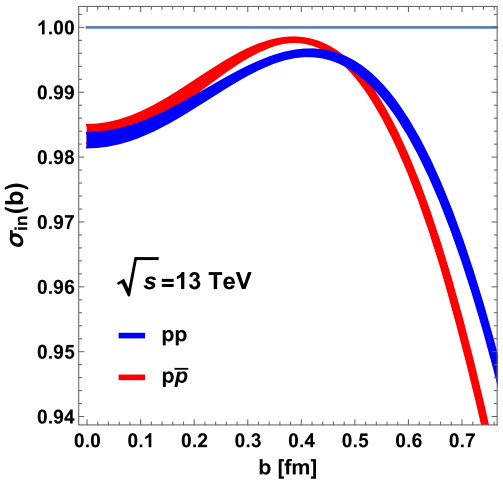

FIG. 7. Close-up of Fig. 6, with visible error bands.

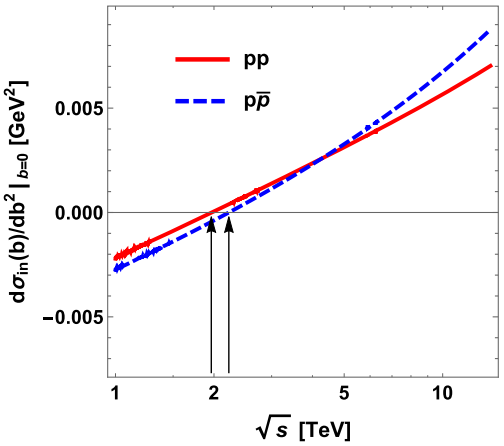

FIG. 8. The criterion for hollowness for pp and $p\bar{p}$, Eq. (16), plotted as a function of the collision energy. Positive values of the curves mean hollowness, with its onset indicated with arrows.

note the feature of hollowness, i.e., a (shallow) minimum in the center. We note that the phenomenon occurs for both pp and $p\bar{p}$ collisions, and is slightly stronger for the latter case. We also display the uncertainty bands corresponding to the error propagation from our fit parameters using the conventional error matrix.[4] As we can clearly see the hollowness is a robust feature as long as the statistical uncertainties are concerned.

From Fig. 8 we see that the onset of hollowness occurs at similar collision energies for pp and for $p\bar{p}$, namely around 3 TeV. However, at higher $\sqrt{s}$ the hollowness becomes somewhat stronger in $p\bar{p}$ compared to pp, as the curvature at the origin is larger for the former case (the dashed curve goes above the solid curve in Fig. 8). This is also manifest in the behavior displayed in Fig. 7.

[4]Namely, for a function $F(p_1, \ldots, p_N)$ of the fitting parameters p_i with correlation matrix $\mathcal{C}_{ij}$ we take $(\Delta F)^2 = \sum_{ij} \mathcal{C}_{ij} \partial_i F \partial_j F$.

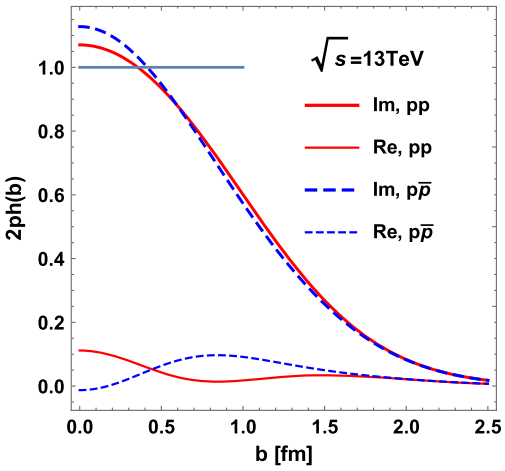

FIG. 9. The real and imaginary parts of the amplitudes $2ph(b,s)$ for pp and $p\bar{p}$, plotted as functions of the impact parameter b for the TOTEM collision energy of $\sqrt{s} = 13$ TeV. We note that near the origin the imaginary parts go above 1.

In the model with strictly linear Regge trajectories the amplitude is a combination of Gaussians in q^2, hence the expression for $2ph(b)$ is analytic, involving a combination of Gaussians in b (with complex parameters). In that case one can write down the criterion of Eq. (16) for hollowness in terms of a relation of the model parameters and s. However, the final formula is long and not very illuminating. A simpler result follows with the condition

$$2p\mathrm{Im}h(s, b = 0) > 1, \tag{40}$$

which becomes equivalent to Eq. (16) in the absence of the real part in the amplitude [17,20]. The behavior of the real and imaginary parts of the elastic amplitude in the b-representation, $2ph(b,s)$, plotted in Fig. 9. We note that near $b = 0$ the imaginary parts go above 1, whereas the real parts are small.

In the model with strictly linear trajectories we find numerically for the dominant component

$$\begin{aligned} 2p\mathrm{Im}h_P(b=0,s) &= \frac{a_P \cos(\frac{\pi\delta_P}{2})(e^{b_P\delta_P} - \epsilon_P)(\frac{s}{s_{P0}})^{\delta_P}}{2b_P s_{P0}\alpha_{P1}} \\ &\simeq 0.64(s/\mathrm{GeV}^2)^{0.028}, \\ 2p\mathrm{Im}h_O(b=0,s) &= \frac{a_O \sin(\frac{\pi\delta_O}{2})(e^{\epsilon_O - b_O\delta_O})(\frac{s}{s_{O0}})^{\delta_O}}{2b_O\alpha_{O1}s_{O1}} \\ &\simeq 0.88(s/\mathrm{GeV}^2)^{0.27}. \end{aligned} \tag{41}$$

The growth with s leads to inevitable crossing of the value 1 at $b = 0$, as seen in Fig. 10.

Finally, we examine condition (29) in our model. The result for the total and 4 times the elastic pp cross sections is displayed in Figs. 11 and 12 for the pp and $p\bar{p}$

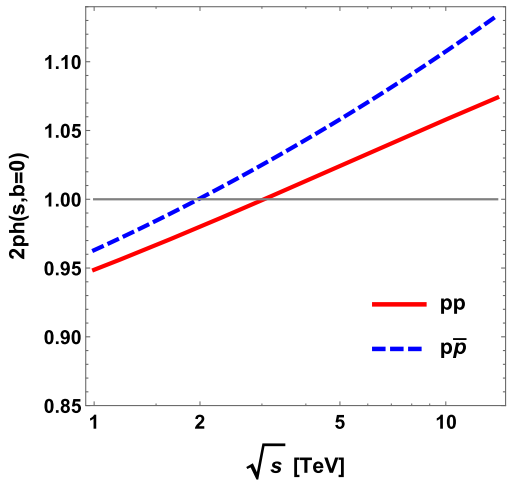

FIG. 10. Value of $2p\mathrm{Im}h$ at the origin, plotted as a function of $\sqrt{s}$. The curves cross the value 1 near the hollowness transition at $\sqrt{s} \sim 3$ TeV.

scattering, respectively. We notice the expected crossing near the hollowness transition, near $\sqrt{s} \sim 3$ TeV.

We have thus demonstrated a firm occurrence of hollowness in the Regge model of Sec. III above $\sqrt{s} \sim 3$ TeV. We have also illustrated the criteria for its appearance. As shown in [17], the very existence of the hollowness phenomenon is quantum-mechanical in nature, as it invalidates folding constructions of the inelasticity profile, as used, e.g., in Refs. [7–12], where hollowness is prevented from the outset.

After this paper was submitted, a work analyzing the overlap function for the pp TOTEM data at the fixed CM energy of 13 TeV [74] was released. It uses the finite binning method suggested in [6], including also error estimates. The results of [74] are compatible with ours,

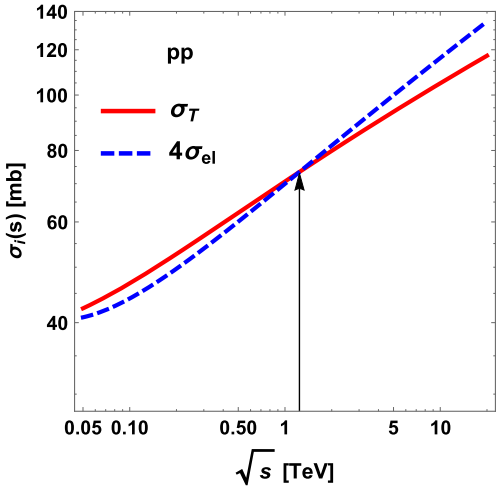

FIG. 11. Comparison of the total and 4 times the elastic pp cross sections, plotted as a function of $\sqrt{s}$. The crossing occurs near the transition to hollowness at $\sqrt{s} \sim 3$ TeV.

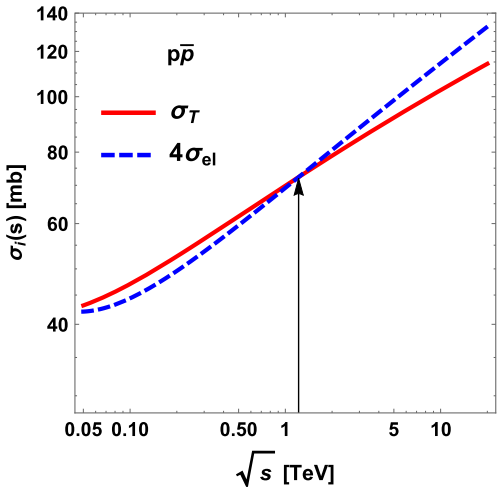

FIG. 12. Same as Fig. 11, but for $p\bar{p}$ scattering

with a clear development of the hollow. We recall that ours is a multi-energy analysis which includes both pp and $p\bar{p}$ within a Regge setup. The persistent occurrence of hollowness at the LHC can be traced to quantum mechanical interference effects which defy purely geometric models [17]. As we have already mentioned, our motivation to use the Regge approach is a realization of analytic properties, such as a fixed-t dispersion relation and crossing, which allows to fix the phase of the amplitude whose absolute value is determined from LHC data. The question whether it is possible or not to redesign a model where analyticity and geometric features are implemented and at the same time data are described, is left for future research.

V. CONCLUSIONS

Over the years, there have been two basic, presumably complementary approaches to the high-energy hadron scattering. The geometric and Regge models rest on different assumptions but they have been implicitly assumed to be dual to each other [1] in the sense that they emphasize the t or s dependence of the scattering amplitude. Based on the results shown in this paper, we argue that this may not necessarily be so, as a simple Regge model fitting globally the pp and $p\bar{p}$ data in a wide energy range displays hollowness at the LHC energies, an effect incompatible with the folding feature characterizing the geometric models [17]. At the same time hollowness is not *a priori* precluded by the Regge theory nor by the fixed-t dispersion relations, and our analysis exemplifies this possibility.

Admittedly, the emergence of hollowness, in pp and $p\bar{p}$ collisions is a remarkable and unexpected feature, unveiling a so far puzzling property which can only stem from a quantum mechanical effect encoded in the amplitude. However, this property cannot be deduced solely from

the elastic scattering data, but needs some theoretical assumptions enabling us to constrain the phase. Our Regge model includes both the Pomeron and the odderon on equal footing, which properly describes the energy- and momentum-transfer dependence in the range from the old ISR to the newest LHC data, and exhibits the phenomenon of hollowness. We have shown that within this framework the onset of hollowness rests mainly on the double-pole Pomeron component. Within the present model we predict the transition region to take place at $\sqrt{s} \sim 3$ TeV, and the feature to hold at all higher energies. Further work is needed to unveil the precise microscopic mechanism behind this emergent and intriguing phenomenon.

ACKNOWLEDGMENTS

This research was supported by the Polish National Science Center, Grant No. 2015/19/B/ST2/00937 (W. B.), by the Spanish Mineco Grants No. FIS2014-59386-P and No. FIS2017-85053-C2-1-P (E. R. A.), by the Junta de Andalucía, Grant No. FQM225-05 (E. R. A.), and by the Ukrainian National Academy's grant "Structure and dynamics of statistic and quantum-mechanical systems" (L. J.).

[1] V. Barone and E. Predazzi, *High-Energy Particle Diffraction* (Springer-Verlag, Berlin, Heidelberg, 2002).
[2] I. M. Dremin, Usp. Fiz. Nauk **183**, 3 (2013) [Phys. Usp. **56**, 3 (2013)].
[3] G. Pancheri and Y. N. Srivastava, Eur. Phys. J. C **77**, 150 (2017).
[4] L. Van Hove, Il Nuovo Cimento **28**, 798 (1963).
[5] L. Van Hove, Rev. Mod. Phys. **36**, 655 (1964).
[6] U. Amaldi and K. R. Schubert, Nucl. Phys. **B166**, 301 (1980).
[7] T. T. Chou and C.-N. Yang, Phys. Rev. **170**, 1591 (1968).
[8] T. T. Chou and C.-N. Yang, Phys. Rev. **175**, 1832 (1968).
[9] H. Cheng and T. T. Wu, *Expanding Protons: Scattering at High Energies* (Mit Press, Cambridge, Massachusetts, 1987).
[10] C. Bourrely, J. Soffer, and T. T. Wu, Phys. Rev. D **19**, 3249 (1979).
[11] M. M. Block, Phys. Rep. **436**, 71 (2006).
[12] M. M. Block, L. Durand, P. Ha, and F. Halzen, Phys. Rev. D **92**, 014030 (2015).
[13] A. Alkin, E. Martynov, O. Kovalenko, and S. M. Troshin, Phys. Rev. D **89**, 091501 (2014).
[14] I. M. Dremin, Kratk. Soobshch. Fiz. **42**, 8 (2015) [Bulletin of the Lebedev Physics Institute **42**, 21 (2015)].
[15] I. M. Dremin, Phys. Usp. **58**, 61 (2015).
[16] E. Ruiz Arriola and W. Broniowski, Few-Body Syst. **57**, 485 (2016).
[17] E. Ruiz Arriola and W. Broniowski, Phys. Rev. D **95**, 074030 (2017).
[18] J. L. Albacete and A. Soto-Ontoso, Phys. Lett. B **770**, 149 (2017).
[19] I. M. Dremin, Phys. Usp. **60**, 333 (2017).
[20] W. Broniowski and E. Ruiz Arriola, Acta Phys. Pol. B **48**, 927 (2017).
[21] I. M. Dremin, arXiv:1702.06304.
[22] V. V. Anisovich, V. A. Nikonov, and J. Nyiri, Phys. Rev. D **90**, 074005 (2014).
[23] S. M. Troshin and N. E. Tyurin, Mod. Phys. Lett. A **31**, 1650079 (2016).
[24] S. M. Troshin and N. E. Tyurin, Eur. Phys. J. A **53**, 57 (2017).
[25] S. M. Troshin and N. E. Tyurin, Int. J. Mod. Phys. A **32**, 1750103 (2017).
[26] L. Puzikov, R. Ryndin, and J. Smorodinsky, Nucl. Phys. **3**, 436 (1957).
[27] V. N. Gribov and D. V. Volkov, Zh. Eksp. Teor. Fiz. **44**, 1068 (1963) [Sov. Phys. JETP **17**, 720 (1963)].
[28] D. H. Sharp and W. G. Wagner, Phys. Rev. **131**, 2226 (1963).
[29] O. V. Selyugin, Phys. Part. Nucl. Lett. **13**, 303 (2016).
[30] A. Gersten, Nucl. Phys. **B12**, 537 (1969).
[31] J. E. Bowcock and H. Burkhardt, Rep. Prog. Phys. **38**, 1099 (1975).
[32] W. Broniowski and E. Ruiz Arriola, Acta Phys. Pol. B Proc. Suppl. **10**, 1203 (2017).
[33] R. J. M. Covolan, J. Montanha, and K. A. Goulianos, Phys. Lett. B **389**, 176 (1996).
[34] R. Phillips and V. D. Barger, Phys. Lett. B **46**, 412 (1973).
[35] D. A. Fagundes, A. Grau, S. Pacetti, G. Pancheri, and Y. N. Srivastava, Phys. Rev. D **88**, 094019 (2013).
[36] J. S. Bell and C. J. Goebel, Phys. Rev. **138**, B1198 (1965).
[37] G. Białkowski, Acta Phys. Pol. B **1**, 109 (1970).
[38] L. L. Jenkovszky and F. Paccanoni, Nuovo Cimento Soc. Ital. Fis. **62A**, 133 (1981).
[39] L. L. Jenkovszky and A. N. Wall, Czech. J. Phys. **26**, 447 (1976).
[40] M. Saleem and F.-e-Aleem, Hadronic J. **5**, 71 (1981).
[41] L. L. Jenkovszky, B. V. Struminsky, and A. N. Shelkovenko, Z. Phys. C **36**, 495 (1987).
[42] L. L. Jenkovszky, E. S. Martynov, and B. V. Struminsky, Phys. Lett. B **249**, 535 (1990).
[43] L. L. Jenkovszky, A. I. Lengyel, and D. I. Lontkovskyi, Int. J. Mod. Phys. A **26**, 4755 (2011).
[44] E. Martynov, Phys. Rev. D **76**, 074030 (2007).
[45] A. Alkin, J. R. Cudell, and E. Martynov, Few-Body Syst. **53**, 87 (2012).
[46] E. Martynov and B. Nicolescu, Phys. Lett. B **778**, 414 (2018).
[47] V. A. Khoze, A. D. Martin, and M. G. Ryskin, Phys. Rev. D **97**, 034019 (2018).

[48] V. A. Khoze, A. D. Martin, and M. G. Ryskin, Phys. Lett. B **780**, 352 (2018).
[49] E. Martynov and B. Nicolescu, Phys. Lett. B **786**, 207 (2018).
[50] J. Kontros, K. Kontros, and A. Lengyel, arXiv:hep-ph/0006141.
[51] J. Kontros, K. Kontros, and A. Lengyel, arXiv:hep-ph/0104133.
[52] A. Wall, L. Jenkovszky, and B. Struminsky, Sov. J. Part. Nucl. **19**, 180 (1988).
[53] G. Antchev *et al.* (TOTEM Collaboration), Europhys. Lett. **101**, 21002 (2013).
[54] The Durham HepData Project, http://durpdg.dur.ac.uk.
[55] P. Abreu *et al.* (Pierre Auger Collaboration), Phys. Rev. Lett. **109**, 062002 (2012).
[56] G. Antchev *et al.* (TOTEM Collaboration), Phys. Rev. Lett. **111**, 012001 (2013).
[57] G. Antchev *et al.* (TOTEM Collaboration), Europhys. Lett. **101**, 21004 (2013).
[58] C. Patrignani *et al.* (Particle Data Group Collaboration), Chin. Phys. C **40**, 100001 (2016).
[59] G. Antchev *et al.* (TOTEM Collaboration), arXiv:1712.06153 [Phys. Rev. D (to be published)].
[60] G. Antchev *et al.* (TOTEM Collaboration), Eur. Phys. J. C **76**, 661 (2016).
[61] G. Antchev *et al.* (TOTEM Collaboration), Report No. CERN-EP-2017-335 [Phys. Rev. (to be published)].
[62] V. Kundrat, M. Lokajicek, and M. V. Lokajicek, Czech. J. Phys. **31**, 1334 (1981).
[63] V. Kundrat and M. Lokajicek, Z. Phys. C **63**, 619 (1994).
[64] J. Prochazka and V. Kundrat, arXiv:1606.09479.
[65] J. Prochazka, V. Kundrat, and M. V. Lokajicek, arXiv:1710.10640.
[66] V. A. Petrov, Eur. Phys. J. C **78**, 221 (2018); **78**, 414(E) (2018).
[67] S. M. Troshin and N. E. Tyurin, Phys. Part. Nucl. **30**, 550 (1999).
[68] J. R. Cudell, E. Predazzi, and O. V. Selyugin, Phys. Rev. D **79**, 034033 (2009).
[69] R. Blankenbecler and M. Goldberger, Phys. Rev. **126**, 766 (1962).
[70] G. L. Pereira da Silva, M. J. Menon, and R. F. Avila, Int. J. Mod. Phys. E **16**, 2923 (2007).
[71] D. A. Fagundes, M. J. Menon, and G. L. P. Silva, Eur. Phys. J. C **71**, 1637 (2011).
[72] O. V. Selyugin, Phys. Rev. D **91**, 113003 (2015); **92**, 099901(E) (2015).
[73] V. A. Petrov and A. P. Samokhin, Int. J. Mod. Phys. Conf. Ser. **47**, 1860097 (2018).
[74] A. Alkin, E. Martynov, O. Kovalenko, and S. M. Troshin, arXiv:1807.06471 [Phys. Rev. D (to be published)].